2024 IEEE International Conference on Robotics and Automation (ICRA)
May 13-17, 2024. Yokohama, Japan

Zero-Shot Wireless Indoor Navigation through Physics-Informed Reinforcement Learning

Mingsheng Yin[1]*, Tao Li[1]*, Haozhe Lei[1]*, Yaqi Hu[1], Sundeep Rangan[1], and Quanyan Zhu[1]

2024 IEEE International Conference on Robotics and Automation (ICRA) | 979-8-3503-8457-4/24/$31.00 ©2024 IEEE | DOI: 10.1109/ICRA57147.2024.10611229

***Abstract*— The growing focus on indoor robot navigation utilizing wireless signals has stemmed from the capability of these signals to capture high-resolution angular and temporal measurements. Prior heuristic-based methods, based on radio frequency (RF) propagation, are intuitive and generalizable across simple scenarios, yet fail to navigate in complex environments. On the other hand, end-to-end (e2e) deep reinforcement learning (RL) can explore a rich class of policies, delivering surprising performance when facing complex wireless environments. However, the price to pay is the astronomical amount of training samples, and the resulting policy, without fine-tuning (zero-shot), is unable to navigate efficiently in new scenarios unseen in the training phase. To equip the navigation agent with sample-efficient learning and zero-shot generalization, this work proposes a novel physics-informed RL (PIRL) where a distance-to-target-based cost (standard in e2e) is augmented with physics-informed reward shaping. The key intuition is that wireless environments vary, but physics laws persist. After learning to utilize the physics information, the agent can transfer this knowledge across different tasks and navigate in an unknown environment without fine-tuning. The proposed PIRL is evaluated using a wireless digital twin (WDT) built upon simulations of a large class of indoor environments from the AI Habitat dataset augmented with electromagnetic radiation simulation for wireless signals. It is shown that the PIRL significantly outperforms both e2e RL and heuristic-based solutions in terms of generalization and performance. Source code is available at `https://github.com/Panshark/PIRL-WIN`.**

I. Introduction

High-frequency transmissions in the millimeter wave (mmWave) bands are a key component of recently developed fifth-generation (5G) wireless systems [1], [2]. In addition to the ability to support massive data rates, the mmWave bands also enable highly accurate positioning and location capabilities [3], [4]. The wide bandwidth of mmWave signals, combined with the use of arrays with large numbers of elements, enables the resolution of paths with high temporal and angular resolution. For robotic navigation and SLAM, mmWave wireless-based positioning can be a valuable complement to camera sensors since the signals can provide information beyond line-of-sight.

This work considers a wireless indoor navigation (**WIN**) problem [5], where a target broadcasts periodic mmWave wireless signals and a mobile robot (agent) has to locate and navigate to the target. Importantly, the environment is initially unknown to the agent. While there has been considerable research on such navigation problems from camera data (see, for example, a survey of deep reinforcement learning methods in [6]), the question is how to leverage the mmWave wireless signals. A growing body of research attempts to address this question [5], [7], [8], where heuristic solutions are developed based on the physics properties of mmWave. For example, [5] presents a simple heuristic navigation strategy based largely on following the angle of arrival (AoA) of wireless signals. This physics-based solution has the advantage that it requires no training and thus does not overfit any specific environment, displaying decent zero-shot generalization. However, this heuristic fails to handle complex wireless environments where mmWave signals propagate along multiple paths through reflections and diffractions [9]. Moreover, observations of these paths are inexact due to noised measurements.

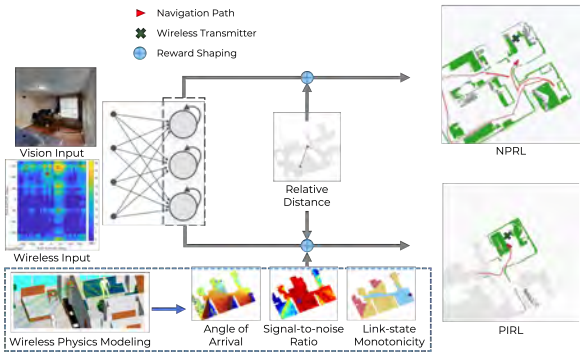

Fig. 1: The wireless indoor navigation (WIN) requires the agent to navigate to the wireless transmitter in an unknown environment using multi-modal input, including vision and wireless. The non-physics e2e RL (NPRL), based on relative distance cost, fails to navigate efficiently in unseen scenarios. Trained to utilize physics prior, physics-informed RL (PIRL) acquires zero-shot generalization with interpretable policies.

When facing such complex indoor navigation tasks, deep reinforcement learning (RL) offers an end-to-end (e2e) learning framework without manual design. Powered by deep representation learning, e2e RL can learn rich policies from complex heterogeneous sensor data. However, such a practice requires hundreds of GPU hours and an exorbitant volume of training data [10]. The resulting policy tends to overfit the training environment, generalizing poorly [11] or requiring pre-exploration when tested in a new environment [8].

To combine the best of two worlds, this work proposes a **physics informed RL** (**PIRL**) approach, training the agent to utilize physics information through reward shaping. As illustrated in Figure 1, the key idea is to use e2e RL but with a relative-distance-based cost function augmented with

[1]Tandon School of Engineering, New York University, NY, USA {my1778, tl2636, hl4155, yh2829, srangan, qz494}@nyu.edu. *These authors contributed equally to this work. Correspondence should be addressed to Tao Li. This work is supported by NSF grants 2133662, 2148293, ECCS-184705, and TIP-2226232.

physically-motivated terms, encouraging the policy to seek actions conforming to physical principles that lead to shorter paths. For the WIN problem, the physical terms include attempts to increase the signal strength, follow the angle of arrival, and navigate to regions where the number of reflections for the strongest path is reduced. Since these physics principles hold across different wireless environments, the proposed PIRL alleviates catastrophic forgetting: previously acquired knowledge is carried over to the ensuing training tasks, leading to sample-efficient learning. Additionally, trained to leverage physics information, the PIRL agent can deal with unseen environments without fine-tuning, achieving zero-shot generalization.

We corroborate the proposed PIRL method using a widely-used AI Habitat indoor navigation dataset [10] combined with detailed RF propagation simulation developed in [5]. This synthesized simulator is referred to as the indoor wireless digital twin (WDT). Our contributions are as below.

1) We propose a physically-motivated reward shaping to achieve physics-informed RL for WIN without map information, enjoying a simple implementation, see (2).
2) We demonstrate that the PIRL requires fewer training samples/resources than vanilla e2e RL does (1593 v.s. 2304 GPU-hours), which is particularly valuable in the WIN problem where wireless simulation is expensive;
3) Our testing experiments show that PIRL generalizes significantly better to new environments in a zero-shot manner, compared with heuristic/RL-based baselines;
4) Inspired by recent advances in explainable AI [12], we conduct sensitivity analysis on the learned PIRL model regarding the input wireless data, showing that the PIRL's actions are interpretable in that they are consistent with physics principles embedded in the reward shaping.

II. Related Work

Our work subscribes to the recent line of research on indoor positioning and localization using high-frequency wireless bands [3]–[5], [8]. Closely related to this work, [5] considers the same WIN setup and proposes a physics-based heuristic: following the AoA, which proves effective in simple scenarios but inadequate when facing complex wireless environments. Similar to our PIRL, [8] develops a deep-learning-based localization algorithm, yet it requires additional map generation for indoor navigation. In contrast, our PIRL incorporates physics knowledge into the RL model, delivering efficient navigation in unexplored environments.

This work also falls within the burgeoning field of physics-informed machine learning, which amounts to introducing appropriate observational, inductive, and learning biases that facilitate the learning process [13]. Our proposed PIRL adopts the last approach: incorporating learning biases, i.e., the physics-motivated reward shaping. By selecting appropriate loss functions to modulate the training, the PIRL favors convergence to solutions adhering to underlying physics. Similar methodologies have been applied to nuclear assembly design [14], aircraft conflict resolution [15], and ramp metering [16]. To the best of our knowledge, this work is among the first endeavors to investigate the physics principles in the 5G wireless domain for RL-based indoor navigation. We refer the reader to Appendix I for an extended discussion[1].

III. Wireless Indoor Navigation: Task Setup

Consider the WIN task setup in [5], where a stationary target is positioned at an unknown location in an indoor environment. The target is equipped with a mmWave transmitter that broadcasts wireless signals at regular intervals. Equipped with a mmWave receiver, an RGB camera, and motion sensors, the agent aims to navigate to the target in minimal time. In contrast to the PointGoal task [17], WIN does not provide the agent with the target coordinates or map information. The detailed environment setup and the agent's actuation/sensor models are provided below.

The agent pose is given by $p = (x, y, \varphi)$ where x, y denotes the xy-coordinate of the agent measured in meters, and φ represents the orientation of the agent in radius (measured counter-clockwise from x-axis). The agent aims to locate and navigate to the target (the wireless transmitter) denoted by (x^*, y^*). We consider a WIN task where the agent operates in the presence of multiple kinds of information feedback that we denote with a vector $o_t = (m_t, \hat{p}_t, v_t, w_t)$, where t is the time step, m_t is an estimate map, $\hat{p}_t = (x_t, y_t)$ is the estimated pose, $v_t = V(p_t)$ represents visual information and $w_t = W(p_t)$ represents the wireless information.

a) Map and Pose: The map and pose estimates can come from any SLAM module. This work uses the state-of-the-art neural SLAM module proposed in [18] that provides robustness to the sensor noise during navigation. This SLAM module internally maintains a spatial map m_t and the agent's pose estimate $\hat{p}_t$ (different from the raw sensor reading $\bar{p}_t$) at each time step during the navigation process. The spatial map is represented as $m_t \in [0,1]^{2\times M\times M}$ is a 2-channel $M \times M$ matrix, where $M \times M$ denotes the map size and each entry corresponds to a cell. Let d denote the width of the map discretization so that each cell is $d \times d$, and the total area is $Md \times Md$, $d = 25\,\mathrm{cm}$. Entries of the first channel of m_t denote the probabilities of obstacles within the corresponding cells, while those of the second channel represent the probabilities of the cells being explored [18].

b) Wireless Information: $W(p) = (g_n, \Omega_n^{rx}, \Omega_n^{tx})_{n=1}^N \in \mathbb{R}^{3\times N}$, where N is the maximum number of detected paths along which signals propagate. For the n-th path, g_n denotes its signal-to-noise ratio (SNR), Ω_n^{rx} and Ω_n^{tx} denote the angle of arrival (AoA) and departure (AoD), respectively. We consider the top $N = 5$ paths with the strongest signal strengths among all paths(see [5] and Appendix VI).

c) Visual Information: $V(p) \in \mathbb{R}^{3\times L_1\times L_2}$ is the 3-channel RGB camera image input at the pose p, where L_1 and L_2 denote the height and the width, respectively. In addition to the wireless sensor and the camera, the agent is also equipped

[1]Appendix is available at https://arxiv.org/abs/2306.06766

with motion sensors. The sensor readings lead to the estimate of the agent pose $\bar{p} = (\bar{x}, \bar{y}, \bar{\varphi})$, which can be different from the agent's authentic pose p. The difference $\varepsilon_{sen} = \bar{p} - p$ is referred to as the sensor noise.

d) Actuation: Following [18], we assume the agent utilizes three default navigation actions, $\mathcal{A} := \{a_F, a_L, a_R\}$. Here, $a_F = (d, 0, 0)$ denotes the moving-forward command with a travel distance equal to the grid size $d = 25\,\mathrm{cm}$; and $a_L = (0, 0, -10^\circ)$ and $a_R = (0, 0, 10^\circ)$ stand for the control commands: turning left and right by 10 degrees, respectively.

IV. Physics-Informed Reinforcement Learning

Navigating within an unknown environment can be viewed as sequential decision-making using partial observations. The agent's state is given by its hidden pose p_t, and only partial information o_t collected by sensors is available at each time step. The state transition is Markovian: $p_{t+1} = p_t + a_t$, $a_t \in \mathcal{A}$. Hence, the WIN task is a partially observable Markov decision process (POMDP), with the observation kernel too complicated to be analytically modeled.

The navigation performance can be measured through a stage cost function defined as the Euclidean distance (or any distance metric, e.g., geodesic distance) between the current pose and the target position $c_t = \|x_t - x^*\|^2 + \|y_t - y^*\|^2$. Denote by $\mathcal{H}_t := \{(o_k, a_k)_{k=1}^{t-1}, o_t\}$ the set of all possible observations up to time t, and by $\mathcal{H} := \cup_{t=1}^{H} \mathcal{H}_t$ the union of all histories, where H denotes the horizon length. The agent's objective is to find an optimal policy $\pi : \mathcal{H} \to \mathcal{A}$ such that the cumulative cost $\mathbb{E}_\pi[\sum_{t=1}^{H} c_t]$ is minimized, implying that the agent navigates to the target in minimal time.

a) Deep RL: The planning algorithms for POMDP [19] are not suitable for WIN, since the state and the observation space are of high dimensions and continuum, and the observation kernel remains unknown. To create model-free learning-based navigation, one can apply deep reinforcement learning, such as proximal policy optimization (PPO) [20], to approximately solve the cost-minimization problem in (1), where the policy π is represented by an actor-critic neural network [21], and its model weights are denoted by $\theta \in \mathbb{R}^d$.

$$\min_\theta \mathcal{L}_{\mathrm{RL}}(\theta) \triangleq \mathbb{E}_{\pi(\theta)} C_{\mathrm{RL}}, \quad C_{\mathrm{RL}} = \sum_{t=1}^{H} c_t, \tag{1}$$

To address the partial observability in WIN, we incorporate a recurrent module [22] into the actor-critic network architecture. With the recurrent neural network (RNN), the policy $\pi(\theta)$ need not take in all past observations $\{(o_k, a_k)_{k=1}^{t-1}, o_t\}$, and instead, the current partial observation suffices, as RNN can memorize historical input and integrate information feedback across time [22]. For more details on the RL implementation, including PPO and RNN, we refer the reader to Appendix III. We refer to RL with the loss function (1) as **non-physics-based RL** (NPRL), to differentiate it from the physics-informed RL to be described shortly.

b) Insufficiency of End-to-End DRL: We observe in the experiments that when NPRL policies are deployed, they exhibit poor generalization ability and sample efficiency. Due to multiple reflections and diffractions of mmWave, the wireless field $W(p)$ changes drastically when the transmitter moves from one location to another, especially when the indoor environment displays complex geometry. Consequently, model weights learned for (overfit) one task are barely relevant to another. In addition to limited generalization, the NPRL agent requires an astronomical amount of samples due to catastrophic forgetting. Since wireless fields vary across different tasks, knowledge of the previously learned task may be abruptly lost when entering into new tasks. Hence, the NPRL agent needs to be re-trained under previous tasks, leading to time-consuming shuffle training [10].

c) Physics-Informed Reinforcement Learning (PIRL): Physics-informed RL (PIRL) or machine learning has emerged as a promising approach to simulate and tackle multiphysics problems in a sample-efficient manner [13]. The gist is that neural networks can be trained from additional information obtained by enforcing physics laws. Existing general-purpose strategies of distilling the physics-domain-knowledge into the RL agent include supervised-learning approaches such as imitation learning [23], and RL approaches such as offline/batch RL [24], [25] and vanilla RL, i.e., online policy learning, where the agent repeatedly interact with the digital twin to acquire feedback. This work considers the simple online learning approach because we need a fair comparison between our proposed PIRL and other baseline wireless navigation approaches that are based on online RL on sample efficiency and generalization.

Adopting online RL, we thus propose to simply augment the cost with *physically-motivated reward shaping* presented in (2), which we denote by $\mathcal{L}_{PIRL}(\theta)$:

$$\mathbb{E}_{\pi(\theta)} \left[C_{\mathrm{RL}} + \lambda_{\mathrm{LS}} C_{\mathrm{LS}} + \lambda_{\mathrm{AoA}} C_{\mathrm{AoA}} + \lambda_{\mathrm{SNR}} C_{\mathrm{SNR}} \right]. \tag{2}$$

The additional terms are motivated by physics principles in WIN: C_{LS}, for link-state monotonicity, C_{AoA} for the angle of arrival direction following, and C_{SNR} for SNR increasing. λ_{LS}, λ_{AoA}, and λ_{SNR} are weighting constants. The following presents the three physics-informed terms.

d) Monotonicity of Link States: In mmWave applications, link states are of great importance [1], [5], which are primarily categorized into Line-of-Sight (LOS) and Non-Line-of-Sight (NLOS). A location (x, y) (or equivalently a pose p) is said to be of LOS if there is a wireless signal path wherein electromagnetic waves traverse from the source to the receiver without encountering any obstacles. In contrast, NLOS signifies the absence of such a direct visual path. NLOS can further be subdivided into first-order, second-order, third-order, and so forth. First-order NLOS (1-NLOS) implies that at least one electromagnetic wave in the wireless link undergoes a single reflection or diffraction. Likewise, second-order NLOS (2-NLOS) suggests at least one electromagnetic wave undergoing two instances of reflection or diffraction. Similar arguments apply to higher-order NLOS, denoted by 2^+-NLOS. Define $\ell(p) \in \{0, 1, 2\}$ as the link state of the pose p, where the link state evaluation 0, 1, and 2 represent the LOS (0-NLOS), 1-NLOS, and 2^+-NLOS

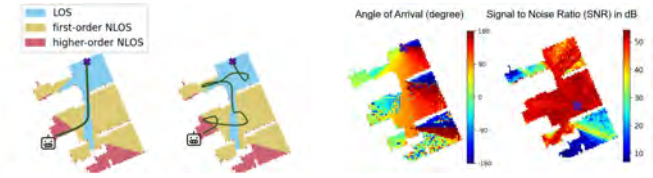

(a) The link state decreases monotonically along the shortest path.

(b) The agent can move reversely along the AoA and explore high SNR area in NLOS.

Fig. 2: The physics principles in WIN.

scenarios, respectively. Note that the link state is a wireless terminology instead of the actual state input to be fed into RL models. Instead, the agent learns to infer the link state from the raw wireless input $W(p)$ [5].

Figure 2a presents a distribution map of link state for indoor wireless signals. The purple cross represents the target location. The LOS coverage, by definition, is a connected area, unlike 1-NLOS, and 2^+-NLOS coverage. Hence, when the agent enters the LOS area, the shortest path to the target is the straight line connecting the two (see Figure 2a), which remains within the LOS area. Another important observation is that the LOS area must be bordered by 1-NLOS, which is then bordered by 2-NLOS, and so forth. In other words, if the link state increases as the agent navigates, the resulting path cannot be optimal. This observation leads to the statement that *a necessary condition for a path to be optimal is that the link state decreases monotonically along the path*, which motivates the term $C_{\mathrm{LS}} = \sum_t \max\{0, \ell_t - \ell_{t-1}\}$.

e) Reversibility of mmWaves: Similar to the principle of reversibility of light, the mmWave follows the same path if the direction of travel is reversed. This reversibility principle leads to a simple yet effective navigation strategy: *following the angle of arrival (AoA) of the strongest path*, which experiences the least number of reflections. Besides, [5] shows that following the AoA of the strongest path in 1-NLOS cases (NLOS with a single reflection) generally leads to decent navigation since it tends to find a route around the obstacle. However, for 2-NLOS cases ($\ell_t = 2$), following the AoA may not be a reliable solution, since it arises from multiple reflections or diffractions. To impose this angle tracking, we add the term $C_{\mathrm{AoA}} = \sum_{t=1}^{H} |\hat{\Omega}_t - \Omega_{1,t}^{rx}|^2 \cdot \mathbb{1}_{\{\ell_t \neq 2\}}$ into (2) where $\hat{\Omega}_t$ is the agent's moving direction derived from the action and $\Omega_{1,t}^{rx}$ is the AoA of the strongest path included in the wireless information w_t.

f) Navigation in 2^+-NLOS: Due to reflections, diffractions, and measurement noises, the reversibility principle is less effective in 2^+-NLOS. Denote by $g(p) = \sum_i g_i(p)$ the overall SNR at the pose p, or equivalently, the location (x, y). A key observation is that g displays remarkable declines in the transit from the LOS and 1-NLOS to 2^+-NLOS areas, see Figure 2b. Upon statistically analyzing 21 maps, it is observed that navigating from the 1-NLOS position to the nearest 2^+-NLOS position leads to an average decline of $25.2\,\mathrm{dB}$ in SNR. Hence, we propose a navigation heuristic in 2^+-NLOS scenarios: the agent should move along the reverse direction of the SNR gradient field $-(\nabla_x g, \nabla_y g)$ (finite differences in practice), i.e., toward the direction with the stronger signal strength. We remark that such a heuristic is less helpful in the LOS and 1-NLOS, where ∇g is relatively insubstantial: the difference between SNRs of two adjacent mesh vertices is mostly within $3\,\mathrm{dB}$. We add the cost $C_{\mathrm{SNR}} = \sum_{t=1}^{H} |\hat{\Omega}_t - \nu_t|^2$ where ν_t denotes the angle between $-\nabla_{x,y} g(p_t)$ and the x-axis. In numerical implementations, ν_t is replaced by the steepest descent direction approximated using finite differences of the mesh points (see Appendix III).

g) Reward shaping and weighting: The negative values of the per-step evaluations of C_{LS}, C_{AoA}, and C_{SNR} are fed to PPO as rewards. The weighting constants λ_{LS}, λ_{AoA}, and λ_{SNR} are properly configured to make the three terms above claim approximately equal shares in (2) so that no one dominates the rest in magnitude. Such an arrangement abides the agent by all physics principles in navigation. The PIRL hyperparameters setup is deferred to Appendix III

h) What does PIRL learn?: One important observation is that the physics-based reward shaping is not a potential-based transformation [26]. To see this, consider a sequence of poses $p_1 \to p_2 \to \cdots \to p_n \to \cdots \to p_1$ such that the agent can travel through them in a cycle, which can incur a net positive cost, e.g., C_{LS} is strictly positive when traversing from LOS to NLOS and then back to LOS. Hence, the policy invariance theorem [26] tells that (2) leads to a navigation policy distinct from the shortest path prescribed by (1). For example, following AoA in the 1-NLOS may yield a detour around a corner rather than the shortest path. Even though PIRL is not optimal, it targets suboptimal solution θ_{PIRL} shared across various tasks (because physics principles are invariant) as shown in Figure 3. The shared suboptimality alleviates catastrophic forgetting in training and creates zero-shot generalization in testing.

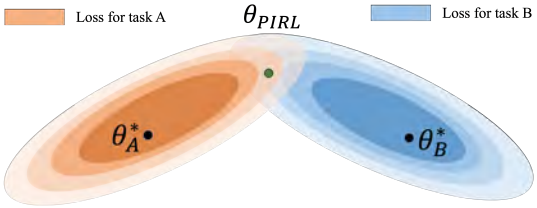

Fig. 3: PIRL targets the suboptimal θ_{PIRL} shared by various tasks, instead of optimal policies θ_A^*, θ_B^* for individual tasks.

V. Experiments

This section evaluates the proposed PIRL approach for WIN tasks, aiming to answer the following questions. 1) **Sample Efficiency**: does the PIRL take fewer training data than the non-physics-based baseline? 2) **Zero-shot Generalization**: can PIRL navigate in unseen wireless environments without fine-tuning? 2) **Interpretablility**: does the PIRL conform to the physics principles, leading to interpretable navigation? We briefly touch upon the training procedure, and the experiment setup in the ensuing paragraph, and details are deferred to Appendix IV. The experiment includes 21 different indoor maps (15 for training; 6 for testing) from the Gibson dataset labeled using the first 21 characters in the Latin alphabet

$(A, B, \ldots, U)$, and each map includes ten different target positions labeled using numbers $(1, 2, \ldots, 10)$. The agent's starting position is fixed for each map regardless of the target position, depending on which, the ten targets for each map are classified into three categories. The first three targets $(1-3)$ are of LOS (i.e., the agent's starting position is within the LOS area), the next three $(4-6)$ belong to 1-NLOS, and the rest four $(7-10)$ correspond to 2^+-NLOS scenarios. For each task (e.g., A1), the maximum number of training episodes is 1000, and the training process terminates if the agent completes the task in more than 6 episodes out of 10 consecutive ones.

We consider three baseline navigation algorithms. 1) non-physics-based RL (NPRL): the RL policy is of the same architecture as our proposed PIRL, whereas the reward function is not physics-informed, i.e., only $\mathcal{L}_{RL}$ in (1). 2) Wireless-assisted navigation (WAN): this non-RL-based method, put forth in [5], relies on a physics-based heuristic that utilizes wireless signals (following AoAs) exclusively within LOS and 1-NLOS scenarios while exploring randomly in 2^+-NLOS. WAN uses a pre-trained classification model to infer the link state. The above two are primarily baselines since our PIRL is a hybrid of the two methodologies. Additionally, to highlight the necessity of leveraging wireless signals in indoor navigation, we consider the third baseline: Vision-augmented SLAM (V-SLAM), which is a vison-augmented version of the active neural SLAM (AN-SLAM) in [18]. V-SLAM only takes in RGB image data without wireless inputs. The V-SLAM agent is capable of localizing the target once it falls within the visual (LOS), whereas in the NLOS, V-SLAM reduces to the AN-SLAM, aiming to explore as much space as possible. Our experiments use the pre-trained vision model and neural-SLAM module.

a) Sample Efficiency: We first evaluate the sample efficiency of the PIRL training process by comparing the number of training episodes of PIRL in LOS, 1-NLOS, and 2^+-NLOS with those of NPRL. The bar plot in Figure 4 gives a visualization of the sample efficiency in the training phase on map A (the first map used in the training) and I (midway in the training). In the early stage of the training, no remarkable difference between the two is observed. Yet, as the training proceeds, PIRL demonstrates a superior sample efficiency on map I, compared with NPRL. This is because the PIRL agent learns to utilize the physics principles that persist across different wireless fields, after being trained on first a few maps. One can see that the PIRL policy already acquires generalization ability to some extent at this point, such that lightweight training would be sufficient for navigating in new environments. In contrast, the NPRL agent, using vanilla end-to-end learning, may be confused when exposed to drastically different wireless fields. Hence, the prior experience does not carry over to the new environment, and NPRL needs to learn almost from scratch.

b) Generalization: We first highlight that our testing environments (new maps with different target positions) are structurally different from training cases. Different room topologies and wireless source locations create drastically different wireless fields unseen in the training phase, as the reflection and diffraction patterns are distinct across each setup. We collect the testing performance of three baselines and our PIRL on maps P to U, and report the average results of 20 repeat tests under different random seeds. Since baselines and PIRL use different reward designs, we consider the metric normalized path length (NPL) defined as the ratio of the actual path length (the number of navigation actions) over the shortest path length of the testing task (the minimal number of actions). The closer NPL is to 1, the more efficient the navigation is. The comprehensive comparison is summarized in Table IV in Appendix V, and Figure 5 gives a visualization of NPLs averaged over the LOS task (e.g. $P1-3$), the 1-NLOS (e.g., $P4-6$), and the 2^+-NLOS (e.g., $P7-10$) on testing maps P and T. Our PIRL policy generalizes well to these unseen tasks and achieves the smallest NPLs across all three scenarios. In addition to NPL, we also report in Figure 5 the Success weighted by (normalized inverse) Path Length (SPL) and in Table I the success rate, which are customary in the literature [17].

TABLE I: Success Rates in Map T and Map P.

		PIRL	NPRL	V-SLAM	WAN
Map T	LOS	1	1	1	1
	1 NLOS	1	1	1	1
	2+NLOS	1	0.4	0.65	0.9
Map P	LOS	1	1	1	1
	1 NLOS	1	1	1	1
	2+NLOS	1	0.45	0.4	0.85

c) Interpretable Navigation: We provide empirical evidence that the PIRL leverages the principles stated in Section IV in the sense that the agent's behavior is well aligned with the physics principles. Specifically, we focus on 1) the reversibility principle: whether the agent follows the AoA, and 2) the gradient heuristic: whether the agent moves toward the high-SNR direction. Figure 6a, 6b, and 6c present the histograms of 1000 sample angle outputs $\hat{\Omega}$ (i.e., moving directions) at a LOS, a 1-NLOS, and a 2^+-NLOS position, respectively. One can see from these figures that the PIRL obeys the physics principles enforced by C_{AoA} and C_{SNR}.

Furthermore, we attempt to interpret the PIRL model using explainable AI methodologies, such as LIME [12]. However, LIME aims to learn an interpretable model (e.g., decision trees) using **perturbed** training data as a surrogate to the original model. The perturbation is to highlight the features contributing the most to the output. The difficulty of applying LIME in WIN setup is that properly perturbing the wireless field is challenging. Due to diffractions and reflections in mmWave propagation, a slight offset to the target location can create drastically different wireless fields. Hence, as a compromise, we compute the gradient of the PIRL model regarding the input wireless data to inspect whether the instrumental features include AoA in LOS/1-NLOS and SNR in 2^+-NLOS, as suggested by the physics principles. Figure 6d, 6e, and 6f empirical confirms that the PIRL model leverages the wireless information as instructed

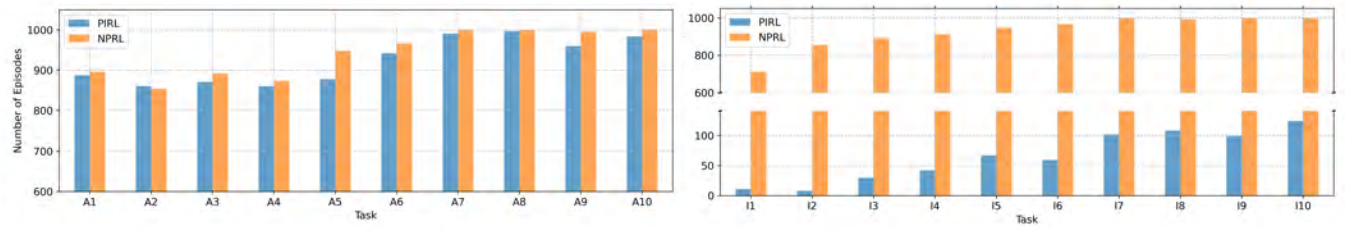

Fig. 4: The number of episodes for ten tasks in map A and I. For each map, task number 1-3, 4-6, and 7-10 are tasks of LOS, 1-NLOS, and 2^+-NLOS case, respectively. Compared with NPRL, PIRL requires fewer and fewer episodes on each case as the training progresses.

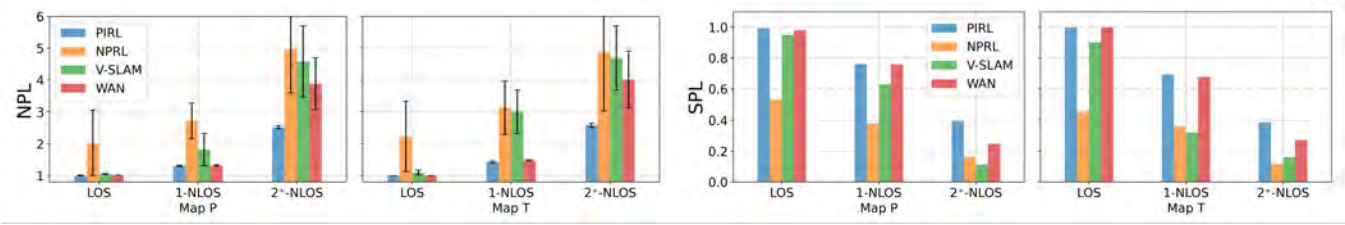

Fig. 5: Average NPLs (left) and SPLs (right) returned by navigation policies in the testing. Unlike NPL, SPL uses the inverse of the path length, and hence, the smaller the SPL one returns, the better it is. Since SPL assign zeros to unsuccessful navigation instances, we do not report its error bar.

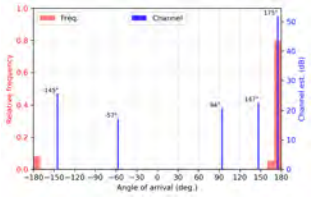

(a) In LOS, PIRL follows the AoA of the first channel (strongest path).

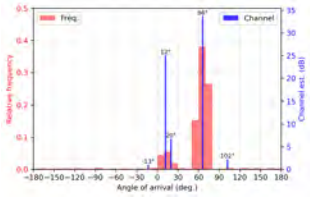

(b) In 1-NLOS, PIRL follows the AoA of the first channel.

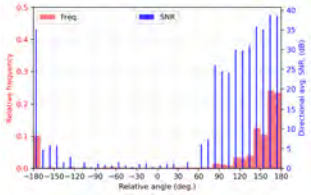

(c) In 2^+-NLOS, PIRL aims at high-SNR directions.

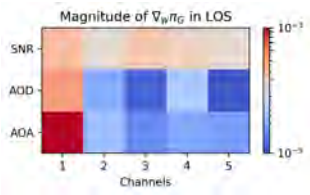

(d) In LOS, the PIRL policy output is mostly sensitive to the AoA of the first channel.

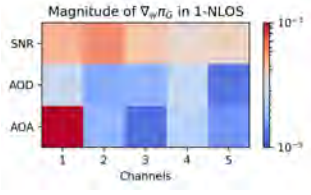

(e) In 1-NLOS, the PIRL policy output is mostly sensitive to the AoA of the first channel.

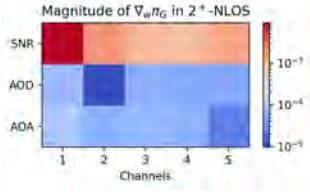

(f) In 2^+-NLOS, the PIRL policy output is mostly sensitive to the SNR of the first channel.

Fig. 6: The interpretability experiments on the reversibility principle and the SNR heuristic.

by the principles, which points to another advantage of incorporating the physics information into RL: the physics-based reward components lead to interpretable navigation.

d) Ablation Study: Recall that PIRL differs from WAN in its use of link state and SNR information. We conduct ablation studies regarding C_{LS} and C_{SNR}, for which we report the NPL results. In the SNR ablation, we replace C_{SNR} with the relative distance cost in 2^+-NLOS to see whether the SNR heuristic helps the agent navigate efficiently in such a scenario. As shown in the third row in Table II, the answer to the question is affirmative, as the SNR ablation returns significantly higher NPLs in 2^+-NLOS. We also suppress C_{LS} to investigate whether the link-state penalty discourages the agent from entering the higher-order NLOS area from the lower-order NLOS. The fourth row in Table II indicates that without C_{LS}, the agent frequently revisits the high-order NLOS areas in testing, yielding higher NPLs in NLOS. In summary, C_{SNR} contributes to PIRL's success in 2^+-NLOS, and C_{LS} helps stabilize the navigation (less variance).

TABLE II: Ablation Studies on the SNR and link state terms. The metric is NPL averaged over all testing tasks.

	LOS	1-NLOS	2^+-NLOS
WAN	1.01 ± 0.01	1.45 ± 0.03	3.83 ± 0.81
PIRL	1.01 ± 0.01	1.41 ± 0.03	2.60 ± 0.05
SNR Ablation	1.02 ± 0.02	1.46 ± 0.04	4.62 ± 1.15
Link State Ablation	1.02 ± 0.02	1.47 ± 0.05	3.90 ± 1.02

VI. Conclusion

This work develops a physics-informed RL (PIRL) for wireless indoor navigation. By incorporating physics prior into reward shaping (RS), PIRL modulates policy learning favoring those adhering to physics principles. As these principles are invariant across training/testing tasks, PIRL alleviates catastrophic forgetting in training and displays zero-shot generalization in testing. One future extension is to symbolize the principles, e.g., using formal methods (more expressive than RS). A synergy of symbolic reasoning and RL would elevate from the data-driven paradigm and create generalizable learning in data-starved situations.

REFERENCES

[1] S. Rangan, T. S. Rappaport, and E. Erkip, "Millimeter-wave cellular wireless networks: Potentials and challenges," *Proceedings of the IEEE*, vol. 102, no. 3, pp. 366–385, 2014.

[2] E. Dahlman, S. Parkvall, and J. Skold, *5G NR: The next generation wireless access technology*. Academic Press, 2020.

[3] A. Shahmansoori, G. E. Garcia, G. Destino, G. Seco-Granados, and H. Wymeersch, "5g position and orientation estimation through millimeter wave mimo," in *2015 IEEE Globecom Workshops (GC Wkshps)*. IEEE, 2015, pp. 1–6.

[4] F. Guidi, A. Guerra, and D. Dardari, "Millimeter-wave massive arrays for indoor slam," in *2014 IEEE International Conference on Communications Workshops (ICC)*. IEEE, 2014, pp. 114–120.

[5] M. Yin, A. K. Veldanda, A. Trivedi, J. Zhang, K. Pfeiffer, Y. Hu, S. Garg, E. Erkip, L. Righetti, and S. Rangan, "Millimeter wave wireless assisted robot navigation with link state classification," *IEEE Open Journal of the Communications Society*, vol. 3, pp. 493–507, 2022.

[6] H. Surmann, C. Jestel, R. Marchel, F. Musberg, H. Elhadj, and M. Ardani, "Deep reinforcement learning for real autonomous mobile robot navigation in indoor environments," *arXiv preprint arXiv:2005.13857*, 2020.

[7] D. Feng, C. Wang, C. He, Y. Zhuang, and X.-G. Xia, "Kalman-filter-based integration of imu and uwb for high-accuracy indoor positioning and navigation," *IEEE Internet of Things Journal*, vol. 7, no. 4, pp. 3133–3146, 2020.

[8] R. Ayyalasomayajula, A. Arun, C. Wu, S. Sharma, A. R. Sethi, D. Vasisht, and D. Bharadia, "Deep learning based wireless localization for indoor navigation," in *Proceedings of the 26th Annual International Conference on Mobile Computing and Networking*, 2020, pp. 1–14.

[9] T. S. Rappaport, R. W. Heath Jr, R. C. Daniels, and J. N. Murdock, *Millimeter wave wireless communications*. Pearson Education, 2015.

[10] M. Savva, A. Kadian, O. Maksymets, Y. Zhao, E. Wijmans, B. Jain, J. Straub, J. Liu, V. Koltun, J. Malik, *et al.*, "Habitat: A platform for embodied AI research," in *Proceedings of the IEEE/CVF international conference on computer vision*, 2019, pp. 9339–9347.

[11] J. Kirkpatrick, R. Pascanu, N. Rabinowitz, J. Veness, G. Desjardins, A. A. Rusu, K. Milan, J. Quan, T. Ramalho, A. Grabska-Barwinska, D. Hassabis, C. Clopath, D. Kumaran, and R. Hadsell, "Overcoming catastrophic forgetting in neural networks," *Proceedings of the National Academy of Sciences*, vol. 114, no. 13, pp. 3521–3526, 2017.

[12] M. T. Ribeiro, S. Singh, and C. Guestrin, ""why should i trust you?": Explaining the predictions of any classifier," in *Proceedings of the 22nd ACM SIGKDD International Conference on Knowledge Discovery and Data Mining*, ser. KDD '16. New York, NY, USA: Association for Computing Machinery, 2016, p. 1135–1144. [Online]. Available: https://doi.org/10.1145/2939672.2939778

[13] G. E. Karniadakis, I. G. Kevrekidis, L. Lu, P. Perdikaris, S. Wang, and L. Yang, "Physics-informed machine learning," *Nature Reviews Physics*, vol. 3, no. 6, pp. 422–440, 2021.

[14] M. I. Radaideh, I. Wolverton, J. Joseph, J. J. Tusar, U. Otgonbaatar, N. Roy, B. Forget, and K. Shirvan, "Physics-informed reinforcement learning optimization of nuclear assembly design," *Nuclear Engineering and Design*, vol. 372, p. 110966, 2021.

[15] P. Zhao and Y. Liu, "Physics Informed Deep Reinforcement Learning for Aircraft Conflict Resolution," *IEEE Transactions on Intelligent Transportation Systems*, vol. 23, no. 7, pp. 8288–8301, 2022.

[16] Y. Han, M. Wang, L. Li, C. Roncoli, J. Gao, and P. Liu, "A physics-informed reinforcement learning-based strategy for local and coordinated ramp metering," *Transportation Research Part C: Emerging Technologies*, vol. 137, p. 103584, 2022.

[17] P. Anderson, A. Chang, D. S. Chaplot, A. Dosovitskiy, S. Gupta, V. Koltun, J. Kosecka, J. Malik, R. Mottaghi, M. Savva, and A. R. Zamir, "On Evaluation of Embodied Navigation Agents," *arXiv*, 2018.

[18] D. S. Chaplot, D. Gandhi, S. Gupta, A. Gupta, and R. Salakhutdinov, "Learning to explore using active neural slam," *arXiv preprint arXiv:2004.05155*, 2020.

[19] H. Kurniawati, "Partially Observable Markov Decision Processes and Robotics," *Annual Review of Control, Robotics, and Autonomous Systems*, vol. 5, no. 1, pp. 1–25, 2022.

[20] J. Schulman, F. Wolski, P. Dhariwal, A. Radford, and O. Klimov, "Proximal policy optimization algorithms," *arXiv preprint arXiv:1707.06347*, 2017.

[21] V. Mnih, A. P. Badia, M. Mirza, A. Graves, T. P. Lillicrap, T. Harley, D. Silver, and K. Kavukcuoglu, "Asynchronous Methods for Deep Reinforcement Learning," 2016.

[22] M. Hausknecht and P. Stone, "Deep recurrent q-learning for partially observable mdps," in *2015 aaai fall symposium series*, 2015.

[23] A. Hussein, M. M. Gaber, E. Elyan, and C. Jayne, "Imitation learning: A survey of learning methods," *ACM Comput. Surv.*, vol. 50, no. 2, apr 2017. [Online]. Available: https://doi.org/10.1145/3054912

[24] J. Bannon, B. Windsor, W. Song, and T. Li, "Causality and Batch Reinforcement Learning: Complementary Approaches To Planning In Unknown Domains," *arXiv preprint arXiv:2006.02579*, 2020.

[25] S. Levine, A. Kumar, G. Tucker, and J. Fu, "Offline Reinforcement Learning: Tutorial, Review, and Perspectives on Open Problems," *arXiv*, 2020.

[26] A. Y. Ng, D. Harada, and S. J. Russell, "Policy invariance under reward transformations: Theory and application to reward shaping," in *Proceedings of the Sixteenth International Conference on Machine Learning*, ser. ICML '99. San Francisco, CA, USA: Morgan Kaufmann Publishers Inc., 1999, p. 278–287.

[27] L. Zwirello, T. Schipper, M. Harter, and T. Zwick, "Uwb localization system for indoor applications: Concept, realization and analysis," *Journal of Electrical and Computer Engineering*, vol. 2012, pp. 1–11, 2012.

[28] T. Li, G. Peng, and Q. Zhu, "Blackwell Online Learning for Markov Decision Processes," *2021 55th Annual Conference on Information Sciences and Systems (CISS)*, vol. 00, pp. 1–6, 2021.

[29] T. Li and Q. Zhu, "On Convergence Rate of Adaptive Multiscale Value Function Approximation for Reinforcement Learning," *2019 IEEE 29th International Workshop on Machine Learning for Signal Processing (MLSP)*, pp. 1–6, 2019.

[30] T. P. Lillicrap, J. J. Hunt, A. Pritzel, N. Heess, T. Erez, Y. Tassa, D. Silver, and D. Wierstra, "Continuous control with deep reinforcement learning," in *4th International Conference on Learning Representations, {ICLR} 2016, San Juan, Puerto Rico, May 2-4, 2016, Conference Track Proceedings*, 2016. [Online]. Available: http://arxiv.org/abs/1509.02971

[31] X.-Y. Liu and J.-X. Wang, "Physics-informed Dyna-style model-based deep reinforcement learning for dynamic control," *Proceedings of the Royal Society A*, vol. 477, no. 2255, p. 20210618, 2021.

[32] J. A. Sethian, "A fast marching level set method for monotonically advancing fronts." *Proceedings of the National Academy of Sciences*, vol. 93, no. 4, pp. 1591–1595, 1996.

[33] K. Cho, B. van Merriënboer, C. Gulcehre, D. Bahdanau, F. Bougares, H. Schwenk, and Y. Bengio, "Learning phrase representations using RNN encoder–decoder for statistical machine translation," in *Proceedings of the 2014 Conference on Empirical Methods in Natural Language Processing (EMNLP)*. Doha, Qatar: Association for Computational Linguistics, Oct. 2014, pp. 1724–1734. [Online]. Available: https://aclanthology.org/D14-1179

[34] K. He, X. Zhang, S. Ren, and J. Sun, "Deep residual learning for image recognition," in *Proceedings of the IEEE Conference on Computer Vision and Pattern Recognition (CVPR)*, June 2016.

[35] B. Han, T. Li, and X. Zhuang, "Directional compactly supported box spline tight framelets with simple geometric structure," *Applied Mathematics Letters*, vol. 91, pp. 213–219, 2019.

[36] C. K. Chui, "Approximations and expansions," in *Encyclopedia of Physical Science and Technology (Third Edition)*, third edition ed., R. A. Meyers, Ed. New York: Academic Press, 2003, pp. 581–607. [Online]. Available: https://www.sciencedirect.com/science/article/pii/B0122274105000260

[37] F. Xia, A. R. Zamir, Z. He, A. Sax, J. Malik, and S. Savarese, "Gibson env: Real-world perception for embodied agents," in *Proceedings of the IEEE conference on computer vision and pattern recognition*, 2018, pp. 9068–9079.

[38] S. Song, F. Yu, A. Zeng, A. X. Chang, M. Savva, and T. Funkhouser, "Semantic scene completion from a single depth image," *Proceedings of 30th IEEE Conference on Computer Vision and Pattern Recognition*, 2017.

[39] "Remcom (accessed on March 10 2022)," available on-line at `https://www.remcom.com/`.

[40] W. Khawaja, O. Ozdemir, and I. Guvenc, "Uav air-to-ground channel characterization for mmwave systems," in *2017 IEEE 86th Vehicular Technology Conference (VTC-Fall)*. IEEE, 2017, pp. 1–5.

[41] Y. Hu, M. Yin, W. Xia, S. Rangan, and M. Mezzavilla, "Multi-frequency channel modeling for millimeter wave and thz wireless communication via generative adversarial networks," *arXiv preprint arXiv:2212.11858*, 2022.

[42] J. Thrane, D. Zibar, and H. L. Christiansen, "Model-aided deep learning method for path loss prediction in mobile communication systems at 2.6 ghz," *Ieee Access*, vol. 8, pp. 7925–7936, 2020.

[43] V. Raghavan, L. Akhoondzadeh-Asl, V. Podshivalov, J. Hulten, M. A. Tassoudji, O. H. Koymen, A. Sampath, and J. Li, "Statistical blockage modeling and robustness of beamforming in millimeter-wave systems," *IEEE Transactions on Microwave Theory and Techniques*, vol. 67, no. 7, pp. 3010–3024, 2019.

[44] J. Song, J. Choi, and D. J. Love, "Codebook design for hybrid beamforming in millimeter wave systems," in *2015 IEEE International Conference on Communications (ICC)*. IEEE, 2015, pp. 1298–1303.

[45] W. Xia, V. Semkin, M. Mezzavilla, G. Loianno, and S. Rangan, "Multi-array designs for mmwave and sub-thz communication to uavs," in *2020 IEEE 21st International Workshop on Signal Processing Advances in Wireless Communications (SPAWC)*. IEEE, 2020, pp. 1–5.

[46] F. Wen, N. Garcia, J. Kulmer, K. Witrisal, and H. Wymeersch, "Tensor decomposition based beamspace esprit for millimeter wave mimo channel estimation," in *2018 IEEE Global Communications Conference (GLOBECOM)*. IEEE, 2018, pp. 1–7.

[47] Z. Zhou, J. Fang, L. Yang, H. Li, Z. Chen, and R. S. Blum, "Low-rank tensor decomposition-aided channel estimation for millimeter wave mimo-ofdm systems," *IEEE Journal on Selected Areas in Communications*, vol. 35, no. 7, pp. 1524–1538, 2017.